

# **Final Project Report**

## **Theoretical and experimental demonstration of broad-angle coupling of Surface Plasmon Polaritons using shaped PDMS prisms**

**Name:** Pierre, Eugene Valassakis

**Student I.D.:** 100004548

**Project Level:** BSc

**Supervisor:** Dr. Andrea Di Falco

**Word Count:** 3905

**Number of pages:** 17

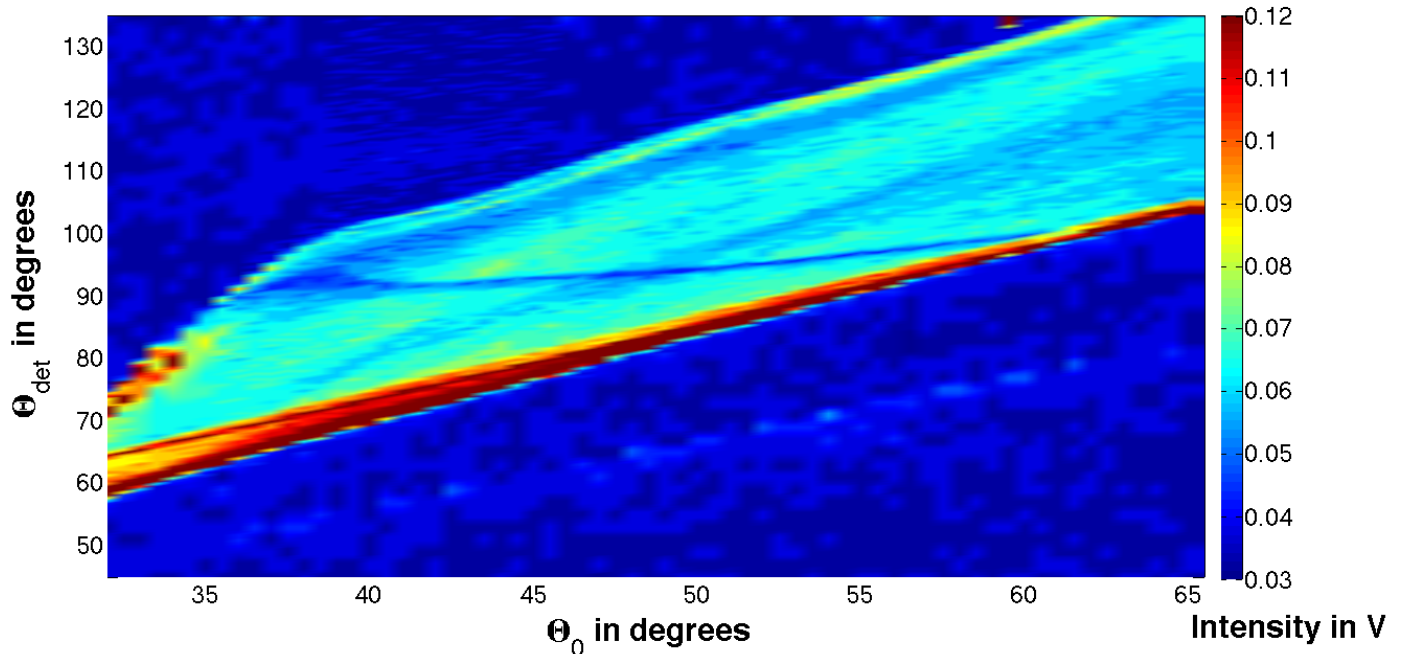
### **Sections:**

<b>Abstract.</b>	<b>2</b>
<b>I. Introduction.</b>	<b>3</b>
<b>II. Theory and Modelling.</b>	<b>4</b>
<b>A. The Model.</b>	<b>4</b>
<b>B. Microscopic systems.</b>	<b>6</b>
<b>III. Experimental Design and Techniques.</b>	<b>7</b>
<b>A. Prism fabrication.</b>	<b>7</b>
<b>B. Characterisation Setup.</b>	<b>8</b>
<b>C. Procedure.</b>	<b>10</b>
<b>IV. Results.</b>	<b>10</b>
<b>V. Discussion.</b>	<b>12</b>
<b>VI. Conclusions.</b>	<b>13</b>
<b>References</b>	<b>14</b>

# **Theoretical and experimental demonstration of broad-angle coupling of Surface Plasmon Polaritons using shaped PDMS prisms**

## **Abstract**

Surface Plasmon Polaritons have been subject of vast research [1] in the past years, and have applications within many fields including Biosensors, Waveguides, SERS, Solar Cells and Data Storage [2-6]. In this letter, we have theoretically and experimentally demonstrated that broad-angle SPP coupling can be achieved using circular PDMS prisms in a Kretschmann-like configuration. In theory, we have predicted that such a coupler should be operational for angles of incidence between  $\sim 0^\circ$ - $80^\circ$ , and we have demonstrated coupling between  $\sim 35^\circ$ - $60^\circ$  experimentally. We also show that these systems could lay the foundation for a scalable configuration allowing broad-angle and broadband coupling on flexible substrates. This is particularly interesting, especially considering the fast growth of the field of flexible electronics [7-18].



*Intensity of the light transmitted from the prism vs. the angle of incidence  $\Theta_0$  and the detector position  $\Theta_{det}$ .*

## **I. Introduction**

Surface Plasmon Polaritons (SPPs) were first detected by Prof. R. W. Wood in 1902, where an “unusual” pattern was detected in the transmitted light when reflected off a metallic grating [2,4,19,20]. Since then, research in the field of Plasmonics has significantly grown [1], driven not only by fundamental science interest in subwavelength optics [2,3,21] but also by its many applications in a wide range of fields from Biosensors to Environmental Science [2-6]. A fundamental feature of SPPs is that they cannot be directly excited by incident light. This is a consequence of their dispersion relation, which lies at the right of the light line of photons in a dielectric medium [2,22,23]. To overcome this fundamental momentum mismatch and couple light with SPPs, many techniques have already been developed [2,22,24-37]. Pioneer work in this matter has been carried out by Kretschmann and Otto, which have used prisms to provide the extra momentum required [24,25]. Other techniques include grating coupling [22,32-37], near field excitation [22,30] or excitation via a highly focussed beam [22,31]. However, most of these techniques have many restrictions, such as relying on rigid/extended systems and/or only achieving coupling for a specific set of parameters (commonly wavelength and angle of incidence) [2,22,24-37]. Developing a configuration where coupling can be achieved

for any angle of incidence/ wavelength and which also displays potential for miniaturisation and flexibility to allow for easy integration into more complex arrangements is therefore highly desirable. A noticeable paper that addresses many of these issues is written by Shulin Sun et al. [38]. In this work, the permittivity and permeability of the coupling surfaces were carefully engineered using a gradually shrinking “H” pattern. This way, a range of momentum increases were available for light to couple to SPPs, and hence the incident wavevector only needed to be smaller than some value  $\xi$ ; ultimately resulting in coupling for any angle above some critical value [38]. However this still relies on the use of complex meta-surfaces and conventional rigid substrates [38]. In this letter, we demonstrate that broad-angle coupling can be achieved using a simple variation of the Kretschmann configuration, using PDMS to form circular prisms. This technique is already used in the industry, as for instance at Biacore Life Sciences [46]. However, there does not seem to be any investigation that uses polymers in such curved prism configurations. The systems considered here then display potential for a much better compatibility with flexible systems, which is desirable as it is in line with the fast development of the field of flexible electronics [7-18]. In our investigation, we model the behaviour of circular PDMS prisms

in regard to coupling, experimentally demonstrate broad-angle SPP excitation, and consider how this configuration could be adapted to the micrometre scale and allow for coupling onto flexible substrates.

## **II. Theoretical Modelling**

### **A. The Model**

In order to give a theoretical basis to the carried work, it is first essential to define the system configuration and parameters. These can be seen in fig.1 below:

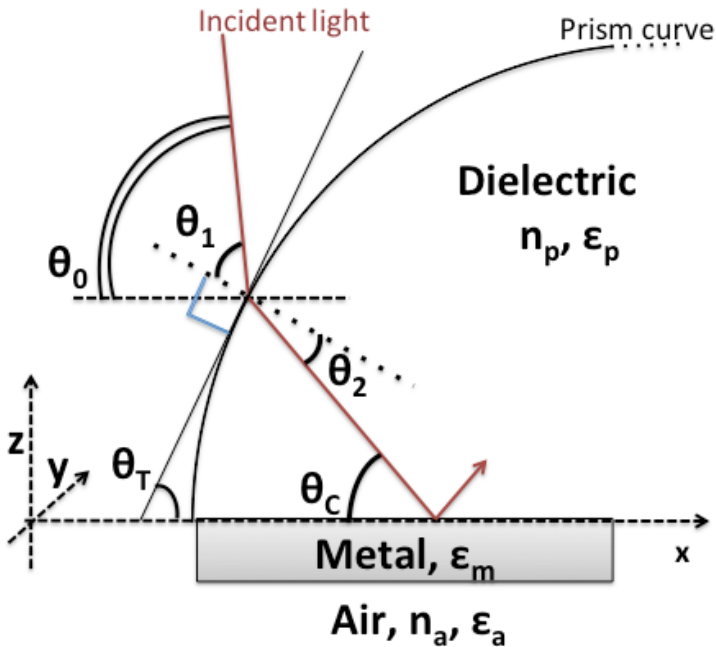


Figure 1. Diagram defining the system configuration and the relevant parameters

A thin metal layer of dielectric constant  $\epsilon_m = n_m^2$  is directly in contact with a prism with  $\epsilon_p = n_p^2$  in a Kretschmann-like configuration [22]. The external environment has a dielectric constant  $\epsilon_a = n_a^2$  and is

considered to be air throughout this paper. The  $x$  direction is taken to be parallel to the metal surface, along the direction of propagation of the plasmon with the origin at the left edge of the prism. The incident light propagates along the  $x$  and  $z$  directions, and is P polarized (with its magnetic field along the  $y$  direction) [2,22]. The angle of incidence  $\theta_0$  is defined to be the angle between the incoming light and the metal surface.  $\theta_1$  is the angle formed between the incident photons and the normal to the surface of the prism and  $\theta_2$  is the corresponding angle within the prism, according to Snell's law [39]. Finally,  $\theta_c$  is the angle at which the light is incident at the metal surface and  $\theta_T$  is the angle between the metal and the tangent to the prism surface at the point of incidence. From geometrical considerations and Snell's law [39], the following of equations are obtained:

$$n_a \sin(\theta_1) = n_p \sin(\theta_2) \quad (1)$$

$$\theta_0 = -\theta_T + \theta_1 + \frac{\pi}{2} \quad (2)$$

$$\theta_2 = \theta_T + \theta_c - \frac{\pi}{2} \quad (3)$$

Solving eq.1,2 and 3 for  $\theta_0$  and eliminating  $\theta_1$  and  $\theta_2$  yields the following:

$$\theta_0 = -\theta_T + \frac{\pi}{2} + \sin^{-1}\left(\frac{n_p}{n_a} \sin\left(\theta_T + \theta_c - \frac{\pi}{2}\right)\right) \quad (4)$$

At this point, it is also important to consider the condition for the incident light to be coupled to SPPs. Within the prism, the  $x$  component of the wavevector of the incident light is  $k_x = n_p k_0 \cos(\theta_c)$ , where  $k_0$  is the

wavevector of the electromagnetic (EM) radiation in vacuum. Equating this to the SPP dispersion relation [2, 22,23],

$$k_x = k_0 \sqrt{\frac{\epsilon_a \epsilon_m}{\epsilon_a + \epsilon_m}} \quad (5)$$

gives the following condition for coupling :

$$\cos(\theta_c) = \sqrt{\frac{\epsilon_a \epsilon_m}{(\epsilon_a + \epsilon_m) \epsilon_p}} \quad (6)$$

Now, adding the condition of eq.6 into eq.4, gives:

$$\theta_0 = -\theta_T + \frac{\pi}{2} + \sin^{-1}\left(\frac{n_p}{n_a} \sin(\theta_T + \cos^{-1} \sqrt{\frac{\epsilon_a \epsilon_m}{(\epsilon_a + \epsilon_m) \epsilon_p}} - \frac{\pi}{2})\right) \quad (7)$$

Eq.7 then yields the angle of incidence  $\theta_0$  that will couple to an SPP for a given slope  $\theta_T$ .

To complete the model, the shape of the prism used is taken to have the functional form  $z = f(x)$ . It is then easy to see that  $\theta_T(x) = \tan^{-1} \left| \frac{df}{dx} \right|$ . Hence, replacing this into eq.7 and letting  $x$  span the length of the prism gives all the values of  $\theta_0$  that will result in coupling to an SPP. The absolute value of the derivative is taken as the systems considered are symmetric, and a negative slope only indicates the outcoupling part of the prism, which is irrelevant here. It is also important to clarify that  $x$  represents the  $x$  coordinate of a point in the surface of the prism, not the point where the light hits the metal surface.

This model was then input into the Maple computational software, using the parameters that correspond to the experiments

performed. A circular dome with unit radius,  $z = f(x) = \sqrt{1^2 - (x - 1)^2}$ , is used for the prism curvature. The prism refractive index is taken to be  $n_p = 1.4295$  [44] and the metal dielectric constant  $\epsilon_m = -18.428$  [40,41] corresponding to PDMS Sylgard 184 and Silver respectively at 635nm. The refractive index of air is considered to be  $n_a = 1.000277$  [42,43].

The curve in fig.2 is then obtained:

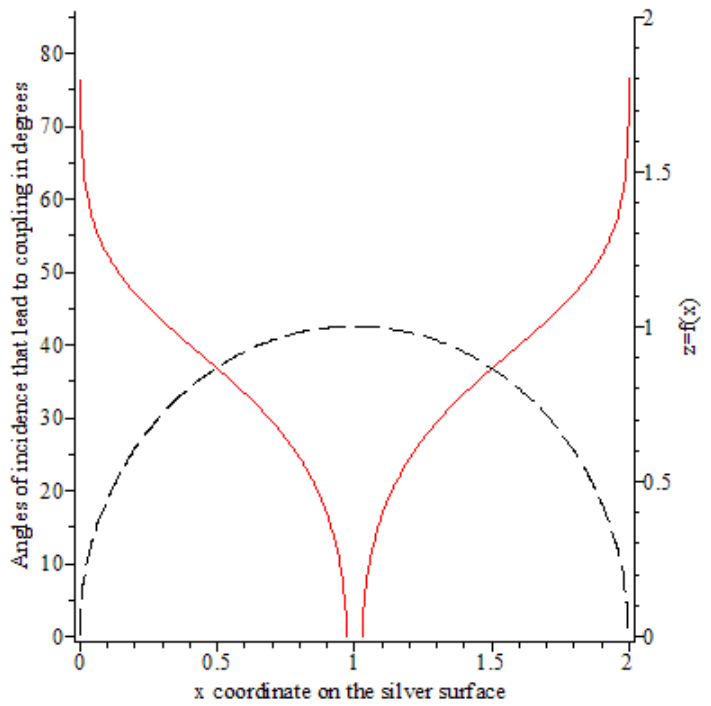


*Figure 2. [solid line] Graphic of the angles of incidence that can theoretically be coupled to SPPs using a single circular PDMS prism of radius 1(the unit here is irrelevant and does not alter the result). [dashed line] Illustration of the circular prism.*

Even though this simulation relies on ideal behaviour of the metal and the dielectric, it clearly indicates that such a system should achieve coupling of light for a range of angles

of incidence between  $\sim 0^\circ$ - $80^\circ$ . It can also be noted that there is a set of slopes at  $x = 1.00 \pm 0.03$  (units here being the same as the units used for the radius) in the middle part of the curvature that do not give rise to coupling, regardless of the angle of incidence considered. In practice, we can reasonably expect a much wider range of slopes around both  $x = 1$  and  $x = 0$  to fail to give coupling, due to edge effects and imperfections. This is quite interesting, as it suggests that one could maximize the efficiency of such systems by carefully engineering the shape of the prisms to reduce the effect of such regions. One way this could be achieved is using the above theory to find a shape  $z = f(x)$  such that  $\theta_0(x)$  is steep around  $x = 0.5$  and levels off around  $x = 0$  and  $x = 1$ .

## **B. Microscopic systems**

In the perspective of achieving broad angle plasmon coupling into microscopic systems and flexible membranes, it is interesting to adapt the model and consider the behaviour of the system upon miniaturisation. In this case, microscopic circular prisms will be arranged in an array with periodicity  $d = 2r$ ,  $r$  being the radius of the prisms. Having the system arranged in such a way further increases the momentum of light due to the periodicity of the prisms. The result is that the  $x$  component

of the wavevector of incident photons is now of the form:

$$k_x = n_p k_0 \cos(\theta_c) + m \frac{2\pi}{d} \quad (8)$$

where  $m$  is an integer. This then changes the condition for coupling to the following:

$$\cos(\theta_c) = \sqrt{\frac{\epsilon_a \epsilon_m}{(\epsilon_a + \epsilon_m) \epsilon_p}} - m \frac{\lambda}{n_p d} \quad (9)$$

The rest of the theory follows naturally in the same way as previously, and allows to determine what angles of incidence can be coupled at a given order  $m$ , and for a given periodicity and wavelength.

Using the analogue of eq.7, which is obtained from the condition in eq.9, a simulation is built into Maple, imputing a periodicity of  $3.5 \mu\text{m}$ . A set of curves analogous to the one in fig.2 is then obtained, each corresponding to a different order  $m$  of momentum increase due to the grading. The results of the simulation are shown in fig.3. Orders higher than those displayed fail to give coupling in this configuration. What this set of curves is indicating is that for each angle of incidence, there will be a discrete set of points in the curvature of the prisms that will allow coupling to occur. This is different from before where only one point had the correct slope to allow for coupling at a given angle of incidence.

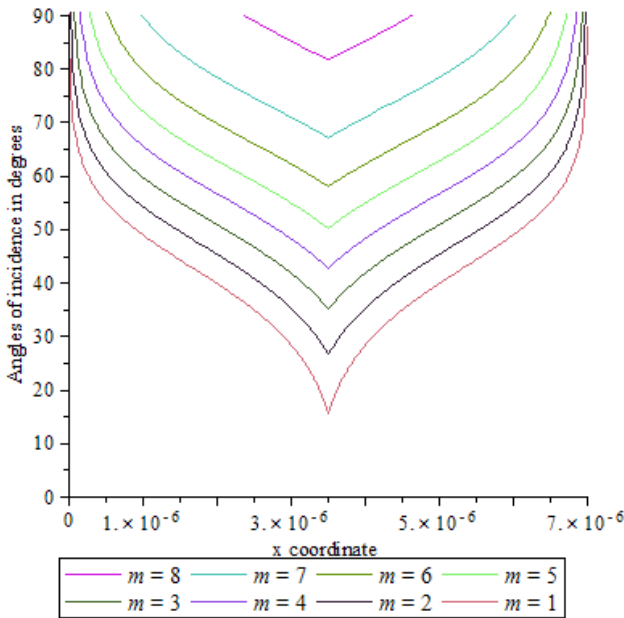


*Figure 3. Angles of incidence that can theoretically be coupled for different orders, considering an array of PDMS prisms with a periodicity of  $3.5\mu\text{m}$ .*

### **III. Experimental Design and Techniques**

#### **A. Prism fabrication**

Using a Computer Aided Design (CAD) program, moulds were designed with the desired circular shape. The radius of the prisms was set to be 1 cm. Moulds for triangular prisms were also fabricated for control purposes. Their design specifications are shown in fig.4,a) and b). Using a 3D printer, the moulds were created with ABS (Acrylonitrile Butadiene Styrene). To obtain optically smooth faces, a three-step process was used. First, the layered pattern on the surfaces inherent to 3D printed objects is eliminated using sand paper. Then the moulds

are immersed for about 15 seconds into Acetone. This melts the surfaces and eliminates most of the defects. Finally, a layer of clear lacquer is applied on the faces to eliminate any remaining roughness. Pictures of the finished moulds can be seen in fig.4,c) and d).

The PDMS used for the prisms was Sylgard 184. It is important to fill the moulds as much as possible in order to prevent at maximum the meniscus formation due to capillary action on the moulds. Also, because of the high viscosity of the PDMS, it can take time for it to fill all the gaps of the moulds, which will decrease the maximum level of the PDMS. After using a desiccator in order to eliminate any air trapped in the PDMS, the samples are baked overnight at  $\sim 45^\circ\text{C}-55^\circ\text{C}$  (to avoid any boiling of the lacquer).

Once the prisms are ready, an electron beam evaporator is used to evaporate 40nm of silver at their base. As PDMS is flexible, obtaining a pristine silver surface without cracks is especially challenging. This point also proved to be critical to the quality of the transmitted beam. To maximize the chances of success, the prisms are demounted and remounted to their own moulds before evaporation. This reduces the grip of the PDMS to its holder, and hence its deformation when it is demounted at the end of the process.

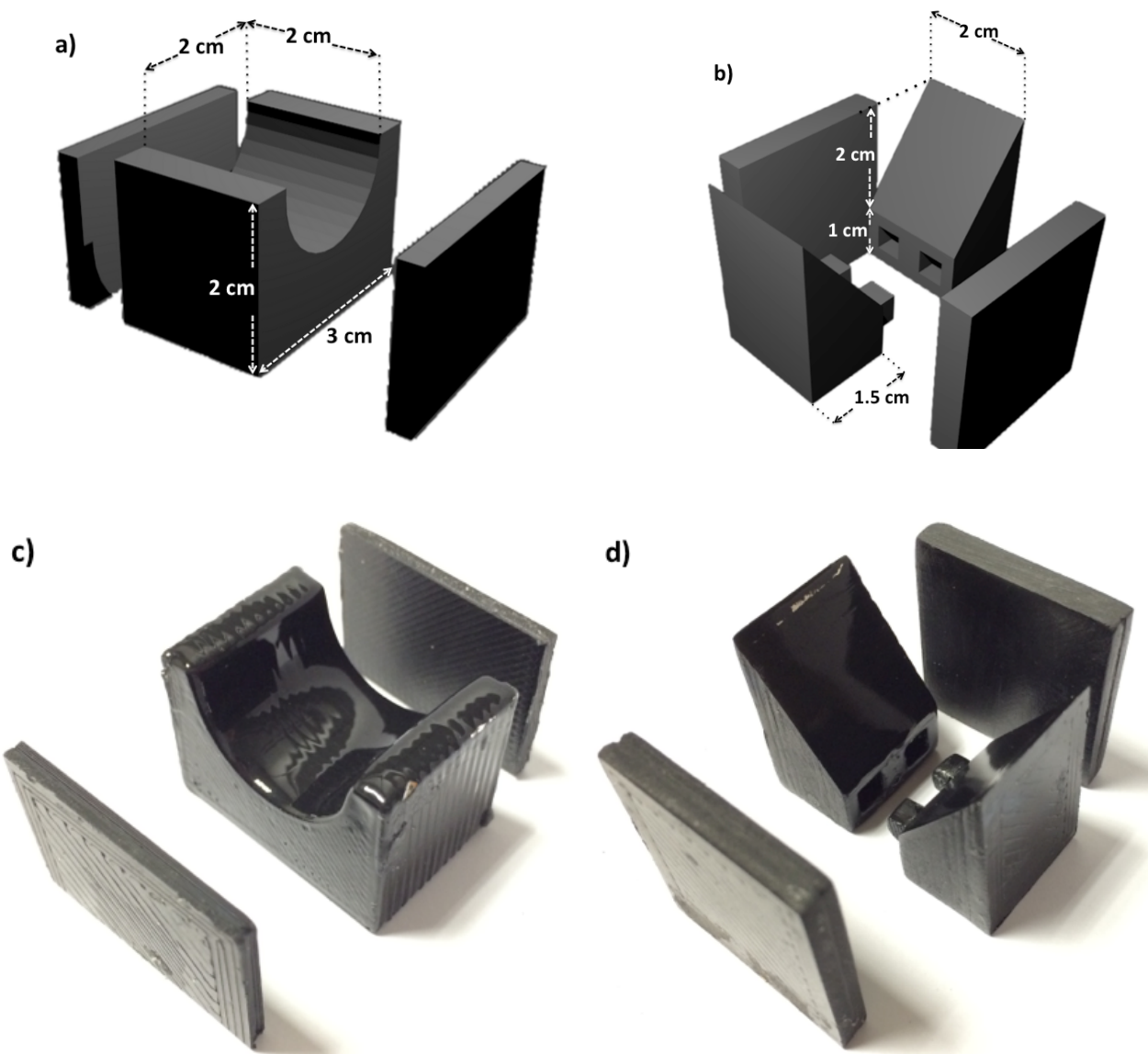


*Figure 4. a), b) Design specifications of the moulds used to create the PDMS prisms. a) Circular prism mould. b) Triangular prism mould, two parts are used to facilitate the sanding process. c), d) Pictures of the moulds created.*

## B. Characterisation Setup

In order to characterise the prisms and their ability to couple plasmons the setup in fig.5 has designed and assembled. The 635nm laser beam is initially focussed with a 60-times-magnification microscope objective with focal

length 2.8 mm. A 100  $\mu\text{m}$  pinhole is placed at the focal point in order to clean the beam. Then, thanks to a  $f_2 = 35 \text{ mm}$  concave lens placed one focal length away from the pinhole, the beam gets collimated and is expanded  $\frac{f_2}{f_1} = 12.5$  times. The result is a beam of  $1.5 \pm 0.1 \text{ cm}$  in diameter. This expansion is

critical as it allows for the majority of the available slopes from the prism's surface to be utilized, which strongly increases the amount of angles that can be coupled. Some drawbacks can also be noted however and really good quality prisms are needed in order to compensate. In particular, the intensity of the beam is reduced dramatically, which makes it much harder to detect and capture features within it; and any defects on the surface become much more problematic as they can't be avoided.

Finally, a polarizer is used such that the light incident on the prisms is P polarized, in order to allow for coupling [2,22]. As a large area

photodetector is used, a  $(1.0 \pm 0.2)mm$  slit is crafted and attached to it, in order to integrate the beam along the z-direction (which does not contain any information). This allows to facilitate the detection of any faint signal, reduces the effect of random fluctuations that are due to defects within the prisms and increases the resolution of the detector (see fig.5). As also shown in fig.5, the angle of incidence  $\theta_0$  is taken to be the angle between the incident beam and the silver surface, which is consistent with our theoretical model above. The detector position  $\theta_{det}$  is taken to be the angle between the incident beam and the detector's axis of rotation.

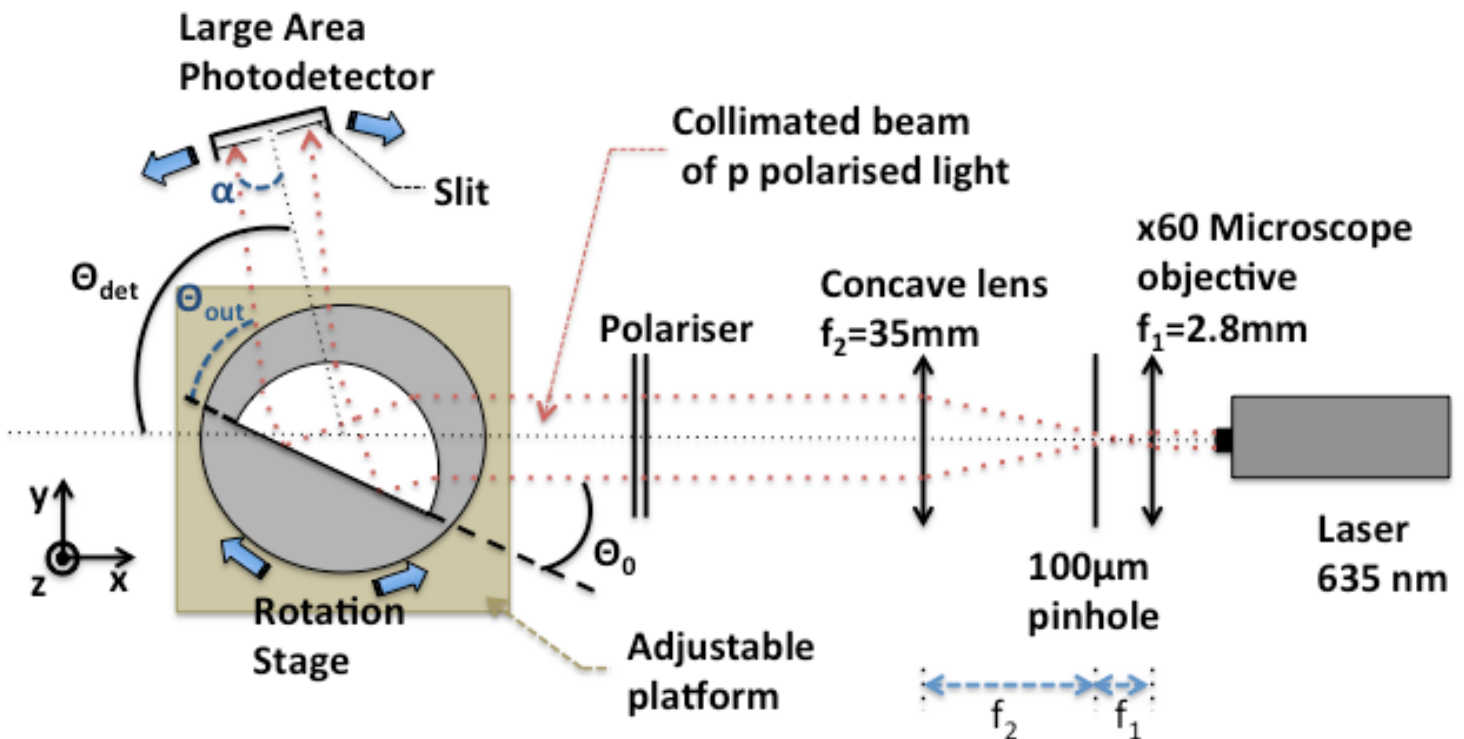


Figure 5. Diagram of the experimental setup used for the characterisation of the prisms.

From fig.5, it is then interesting to note that

$$\theta_{det} = \alpha + \theta_0 + \theta_{out} \quad (10)$$

In eq.10, and as can be seen in fig.5,  $\alpha$  depends on the position of the prism with respect to the centre of rotation of the rotation stage. Also, in the triangular prism case  $\theta_0 = \theta_{out}$  and hence eq.10 becomes:

$$\theta_{det} = \alpha + 2\theta_0 \quad (11)$$

### C. Procedure

The appropriate prism is placed on the rotation stage, which is then aligned such that the transmitted light always hits the detector. The setup is then calibrated by setting the positions  $\theta_0 = 0^\circ$  and  $\theta_{det} = 0^\circ$ . The intensity due to background noise is also assessed to be  $I_0 = 0.0356 V$  by taking intensity measurements at several detector positions with the laser off, and then averaging the obtained values.

For the data acquisition, the intensity incident on the detector is measured as a function of  $\theta_{det}$ , at a fixed  $\theta_0$ . Then  $\theta_0$  is varied and the process is repeated. The majority of this procedure is then automated thanks to Labview programing, making it quite easy to collect the necessary data to a fairly good level of precision.

### IV. Results

The prisms obtained and the corresponding data gathered are illustrated in fig.6. The triangular prism follows a standard Kretschmann configuration and is used as a control experiment. The data gathered are plotted in fig.6,b) and d).

It is first relevant review the results for the triangular prism. As can be seen from fig.6,b), the features of the experimental data are fairly close to those expected in theory. There are however some noticeable differences. In an ideal setup, the plasmon extinction should appear in the form of the lines l1 for a PDMS refractive index  $n_p = 1.4295$  (value quoted by Florian Schneider et al. [44]), and l2 for  $n_p = 1.41$ . As PDMS is obtained through mixing a base and a curing agent together, it does not seem unreasonable that its refractive index changes for each sample created. This could then explain why we observe coupling around l2 rather than l1 in this case. Another observation is that the experimental beam is shifted to slightly higher  $\theta_{det}$  values compared to the ideal case, a systematic error that naturally occurs in terms of eq.10 and 11.

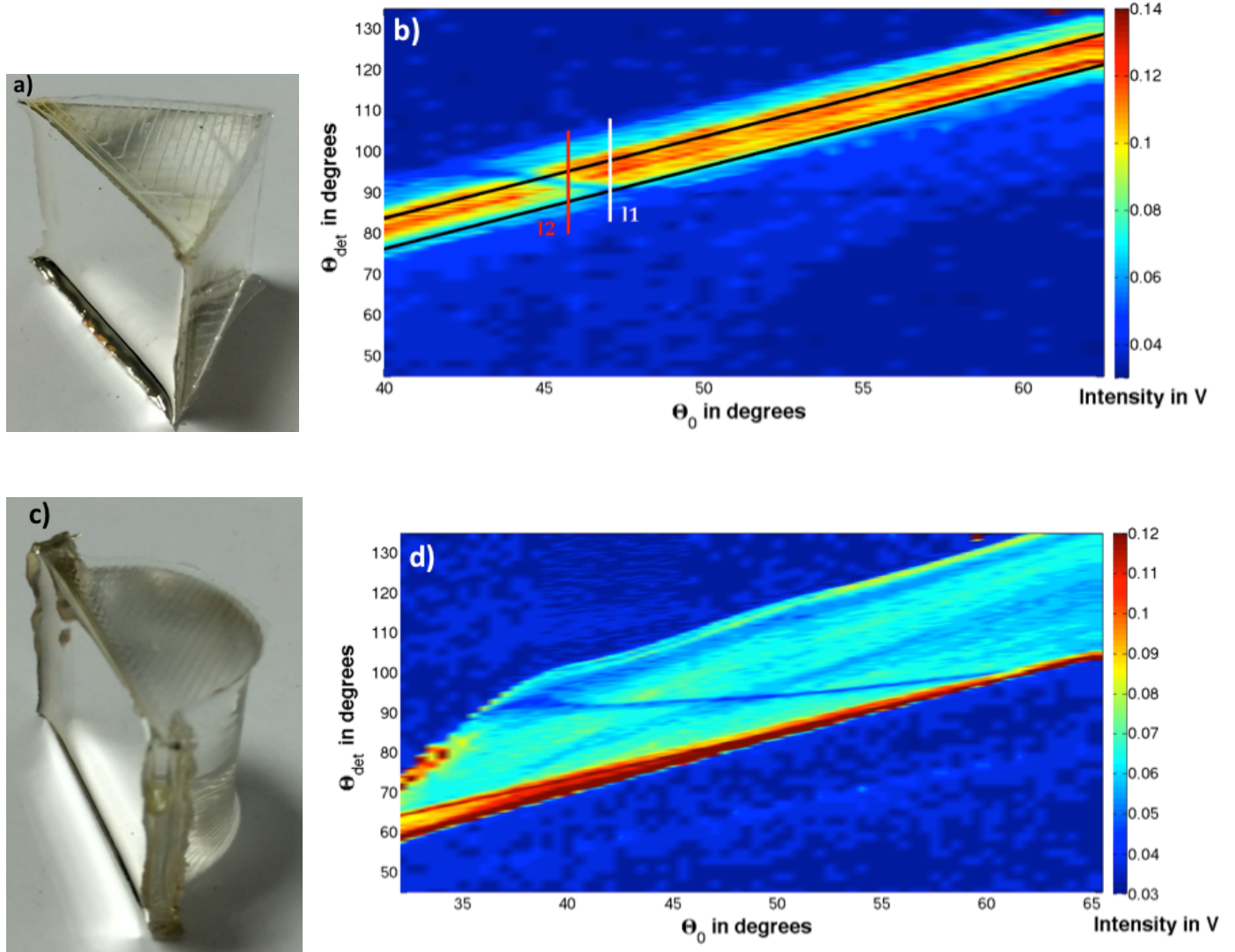


*Figure 6. a) Picture of the triangular prism. b) Intensity at the detector vs. the detector position and the angle of incidence for the triangular prism. I1 represents how the plasmon extinction should appear for  $n_p = 1.4295$  in a perfect Kretschmann configuration. I2 represents the corresponding plasmon extinction if  $n_p = 1.41$ . The other two parallel lines represent where the beam should appear in an ideal setup. c) Picture of the circular prism. d) Intensity at the detector vs. the detector position and the angle of incidence for the circular prism.*

One more troubling feature is that we can clearly detect coupling for angles between  $\sim 43^\circ$ - $48^\circ$ . In theory, coupling should only occur at  $\sim 45.7^\circ$  (for  $n_p = 1.41$ ), and the extinction line should be vertical, as can be

seen in fig.6,b). This can be accounted for by considering fig.6,a), where it is visible that the silver surface is not entirely flat, but takes in fact the form of the meniscus formed by the PDMS within its mould. This then

automatically provides a range of angles of incidence on the silver surface, or equivalently a range of momentum increases that photons can use to couple to SPPS.

It is important to then keep these effects in mind when interpreting the data obtained for the circular prism. The first thing to notice while looking at fig.6,d) is that we are clearly getting a significantly higher range of coupling angles, namely  $\sim 35^\circ$ - $60^\circ$ . For this configuration, the light is incident on a range of points on the silver surface and with a range of different angles, and the beam in most cases does not stay collimated, making it substantially more complex to model mathematically its behaviour and predict exact features. Several qualitative arguments can however be made.

The higher intensity values that are visible at the lower part of the beam in fig.6,d) are likely to be due to direct reflections and scattering of light off the corners formed at the edges of the circular part of the prism (see fig.6,c)).

Even though quite wide, the range of incidence angles that are coupled is smaller than the theoretical predictions. It is also observed that the plasmon is coupled on the silver surface at points between  $(3.0 \pm 1.5) \text{ mm}$  and  $(5.0 \pm 1.5) \text{ mm}$  off each edge of the prism. Using our theoretical model, and adjusting for the  $2\text{mm} \pm 1\text{mm}$  base of our prism (see fig.6,c)); it is predicted that for an angle of

incidence of  $60^\circ$  (the maximum angle for which we observe coupling), the plasmon should be excited at  $0.476 \text{ cm}$  off one edge of the prism and for an angle of incidence of  $35^\circ$  it should be excited at  $0.312 \text{ cm}$  off the other edge. These values are in agreement within uncertainties with our experimental values, which demonstrates some robustness for our model. It is then sensible to account for the reduced range of coupling angles with imperfections linked to edge effects. These could be a less smooth silver surface, the curvature of the silver due to the meniscus effect which is more pronounced towards the edges or reflection/scattering off the corner at the boundary between the base and the bulk parts of the prism (see fig.6,a)).

## V. Discussion

By comparing the results obtained from the triangular prism and the circular one, it is clearly apparent that the circular prism is able to achieve coupling for a much wider range of angles. This constitutes a clear proof of concept, even though many secondary effects that are hard to quantify are present. To improve the results, the next step would involve finding ways to reduce the meniscus shape of the silver surface. One possibility would be to include the prisms into frames that would force the surface flat. This would however require very careful handling not to

crack the silver surface, and would increase the complexity and rigidity of the system, which could be a disadvantage in the context of integrating the prisms into larger structures. Another possibility would be to redesign the moulds such that they are capped. Once filled with PDMS, one could add the cap on top such that the PDMS takes up all the available space, not allowing for capillary effects. In that case a different, more thermally conducting material could be more appropriate to make the moulds, considering the baking step during the fabrication. This is nevertheless not a requirement, as in any case PDMS is able to solidify even without being baked, with the process just being slower.

Regarding the theory, further development would include taking into account damping due to real metal and dielectric behaviour. This is possible by considering the full complex dielectric functions of the materials [22,45]

$$\varepsilon_m = \varepsilon_{m1} + \varepsilon_{m2}i \quad (10)$$

and

$$\varepsilon_p = \varepsilon_{p1} + \varepsilon_{p2}i \quad (11)$$

In this case, one would need to consider the real parts of the wavevectors in deriving eq.7 [22], and also proceed with care in the application of Snell's law to determine the direction of refracted light [45]. This would then allow for a better understanding and therefore control over the prisms behaviour.

Also, if the full dependence on frequency of the dielectric functions is obtained, one will be able to model for broadband coupling, predicting coupling properties of the prisms at any wavelength.

Finally, the natural extension of this work is to scale down the size of the prisms to the micrometre level and use them in an array to couple light. As the material used is PDMS, the resulting membrane should be a flexible, broad angle, and potentially broadband, coupler of SPPs. Using the theory we developed for this case, we predict that this will produce a series of extinction lines on the transmitted beam for each angle of incidence, each one corresponding to a different order  $m$ . Such a system would then also display potential to couple while bended, which is a quite desirable and novel feature.

## **VI. Conclusions**

We have demonstrated the ability of circular PDMS prisms to achieve broad-angle coupling of SPPs both theoretically and experimentally. In an ideal theoretical system, and for a 635nm wavelength, such prisms should achieve coupling for incidence angles ranging from  $0^\circ$  to more than  $80^\circ$ . In practice, we have observed coupling at angles between  $\sim 35^\circ$ - $60^\circ$ , and attributed this reduced range to the meniscus formed on the silver surface and

other edge effects that occur in the real systems. We have also theoretically and conceptually investigated a thin membrane composed of an array of microscopic circular prisms; predicting that in such a configuration several extinction lines should be seen in the transmitted beam. Extensions of these investigations follow naturally, namely testing the prism's ability to couple plasmons for other than 635nm wavelengths; and creating and characterising thin, flexible PDMS membranes composed of an array of microscopic circular prisms. Such systems then have the potential to evolve into highly efficient, non-restrictive (in angle or in wavelength), flexible and scalable SPP couplers, with applications in a variety of fields as Biosensors, Solar cells, Data Storage and flexible Optoelectronics [2-6].

## References

- [1] UCD Plasmonics, Plasmonics and Ultrafast NanoOptics. n.d. *Surface Plasmons- a Brief History, Adapted from the Phd Thesis of Brian Ashall..* [online] Available at: [http://www.ucd.ie/biophysics/sp\\_history.htm](http://www.ucd.ie/biophysics/sp_history.htm) [Accessed: 21 April 2014].
- [2] Zhang, J., Zhang, L. and Xu, W. 2012. Surface plasmon polaritons: physics and applications. *Journal of Physics D: Applied Physics*, 45 (11), p. 113001.
- [3] Zayats, A. V., Smolyaninov, I. I. and Maradudin, A. A. 2005. Nano-optics of surface plasmon polaritons. *Physics reports*, 408 (3), pp. 131--314.
- [4] Nicolas BONOD, Surface Plasmons: fundamentals and applications for photovoltaic cells, FrontNanoSpinPhoto conference presentation, available at: <http://www.cinam.univ-mrs.fr/confs/FrontNanoSpinPhoto/PDF/BOND.pdf> (November 17-19, 2009).
- [5] Maier, S. A., Brongersma, M. L., Kik, P. G., Meltzer, S., Requicha, A. A. and Atwater, H. A. 2001. Plasmonics\ DHA Route to Nanoscale Optical Devices\*. *Adv. Mater*, 13 (19), p. 2.
- [6] Daghestani, H. N. and Day, B. W. 2010. Theory and applications of surface plasmon resonance, resonant mirror, resonant waveguide grating, and dual polarization interferometry biosensors. *Sensors*, 10 (11), pp. 9630--9646.
- [7] Kim, D., Kim, Y., Wu, J., Liu, Z., Song, J., Kim, H., Huang, Y. Y., Hwang, K. and Rogers, J. A. 2009. Ultrathin Silicon Circuits With Strain-Isolation Layers and Mesh Layouts for High-Performance Electronics on Fabric, Vinyl, Leather, and Paper. *Advanced Materials*, 21 (36), pp. 3703--3707.
- [8] Rogers, J. A., Someya, T. and Huang, Y. 2010. Materials and mechanics for stretchable electronics. *Science*, 327 (5973), pp. 1603--1607.

- [9] Sun, Y. and Rogers, J. A. 2007. Inorganic semiconductors for flexible electronics. *Advanced Materials*, 19 (15), pp. 1897--1916.
- [10] Sun, Y., Choi, W. M., Jiang, H., Huang, Y. Y. and Rogers, J. A. 2006. Controlled buckling of semiconductor nanoribbons for stretchable electronics. *Nature nanotechnology*, 1 (3), pp. 201--207.
- [11] Sekitani, T., Noguchi, Y., Hata, K., Fukushima, T., Aida, T. and Someya, T. 2008. A rubberlike stretchable active matrix using elastic conductors. *Science*, 321 (5895), pp. 1468--1472.
- [12] Sekitani, T., Zschieschang, U., Klauk, H. and Someya, T. 2010. Flexible organic transistors and circuits with extreme bending stability. *Nature materials*, 9 (12), pp. 1015--1022.
- [13] Someya, T., Kato, Y., Sekitani, T., Iba, S., Noguchi, Y., Murase, Y., Kawaguchi, H. and Sakurai, T. 2005. Conformable, flexible, large-area networks of pressure and thermal sensors with organic transistor active matrixes. *Proceedings of the National Academy of Sciences of the United States of America*, 102 (35), pp. 12321--12325.
- [14] Ko, H. C., Shin, G., Wang, S., Stoykovich, M. P., Lee, J. W., Kim, D., Ha, J. S., Huang, Y., Hwang, K. and Rogers, J. A. 2009. Curvilinear electronics formed using silicon membrane circuits and elastomeric transfer elements. *Small*, 5 (23), pp. 2703--2709.
- [15] Sekitani, T. and Someya, T. 2010. Stretchable, Large-area Organic Electronics. *Advanced Materials*, 22 (20), pp. 2228--2246.
- [16] Klauk, H., Halik, M., Zschieschang, U., Eder, F., Rohde, D., Schmid, G. and Dehm, C. 2005. Flexible organic complementary circuits. *Electron Devices, IEEE Transactions on*, 52 (4), pp. 618--622.
- [17] Mannsfeld, S. C., Tee, B. C., Stoltenberg, R., Chen, C. V. H., Barman, S., Muir, B. V., Sokolov, A. N., Reese, C. and Bao, Z. 2010. Highly sensitive flexible pressure sensors with microstructured rubber dielectric layers. *Nature materials*, 9 (10), pp. 859--864.
- [18] Aksu, S., Huang, M., Artar, A., Yanik, A. A., Selvarasah, S., Dokmeci, M. R. and Altug, H. 2011. Flexible plasmonics on unconventional and nonplanar substrates. *Advanced Materials*, 23 (38), pp. 4422--4430.
- [19] Wood, R. W. 1902. On a Remarkable Case of Uneven Distribution of Light in a Diffraction Grating Spectrum. *Proceedings of the Physical Society of London*, 18 (1), p. 269.
- [20] Wood, R. 1912. XXVII. Diffraction gratings with controlled groove form and abnormal distribution of intensity. *Philosophical Magazine Series 6*, 23 (134), pp. 310-317.
- [21] Barnes, W. L., Dereux, A. and Ebbesen, T. W. 2003. Surface plasmon subwavelength optics. *Nature*, 424 pp. 824-830.
- [22] Maier, S. A. 2007. *Plasmonics: Fundamentals and Applications*. [New York]: Springer Science+Business Media, LLC. pp. 5-52

- [23] Humboldt-Universitat zu Berlin, Olivier Benson, Chapter 7: Plasmonics, available through <http://www.physik.hu-berlin.de/nano/lehre/Gastvorlesung%20Wien/> or directly at <http://www.physik.hu-berlin.de/nano/lehre/Gastvorlesung%20Wien/plasmonics> [visited 21 April 2014].
- [24] Otto, A. 1968. Excitation of nonradiative surface plasma waves in silver by the method of frustrated total reflection. *Zeitschrift f\ "ur Physik*, 216 (4), pp. 398--410.
- [25] Kretschmann, E. and Reather, H. 1968. Radiative decay of nonradiative surface plasmon excited by light. *Z. Naturf.*, 23A p. 2135.
- [26] Wang, H. 1995. Coupling to surface plasmon waves by the use of a birefringent prism coupler. *Optics communications*, 119 (1), pp. 75--77.
- [27] O'hara, J., Averitt, R. and Taylor, A. 2005. Prism coupling to terahertz surface plasmon polaritons. *Optics express*, 13 (16), pp. 6117--6126.
- [28] Kan, T., Tsujiuchi, N., Iwase, E., Matsumoto, K. and Shimoyama, I. 2010. Planar near-infrared surface plasmon resonance sensor with Si prism and grating coupler. *Sensors and Actuators B: Chemical*, 144 (1), pp. 295-300.
- [29] Charbonneau, R., Lisicka-Shrzek, E. and Berini, P. 2008. Broadside coupling to long-range surface plasmons using an angle-cleaved optical fiber. *Applied Physics Letters*, 92 (10), pp. 101102--101102.
- [30] Hecht, B., Bielefeldt, H., Novotny, L., Inouye, Y. and Pohl, D. 1996. Local excitation, scattering, and interference of surface plasmons. *Physical Review Letters*, 77 (9), p. 1889.
- [31] Bouhelier, A. and Wiederrecht, G. 2005. Excitation of broadband surface plasmon polaritons: Plasmonic continuum spectroscopy. *Physical Review B*, 71 (19), p. 195406.
- [32] Devaux, E., Ebbesen, T. W., Weeber, J. and Dereux, A. 2003. Launching and decoupling surface plasmons via micro-gratings. *Applied physics letters*, 83 (24), pp. 4936--4938.
- [33] Hooper, I. R. and Sambles, J. R. 2003. Surface plasmon polaritons on thin-slab metal gratings. *Physical Review B*, 67 (23), p. 235404.
- [34] Cesario, J., Quidant, R., Badenes, G. and Enoch, S. 2005. Electromagnetic coupling between a metal nanoparticle grating and a metallic surface. *Optics letters*, 30 (24), pp. 3404--3406.
- [35] Chen, C. and Berini, P. 2010. Grating couplers for broadside input and output coupling of long-range surface plasmons. *Optics Express*, 18 (8), pp. 8006--8018.
- [36] Offerhaus, H., Van Den Bergen, B., Escalante, M., Segerink, F., Korterik, J. and Van Hulst, N. 2005. Creating focused plasmons by noncollinear phasematching on functional gratings. *Nano letters*, 5 (11), pp. 2144--2148.
- [37] Ritchie, R., Arakawa, E., Cowan, J. and

- Hamm, R. 1968. Surface-plasmon resonance effect in grating diffraction. *Physical Review Letters*, 21 (22), p. 1530.
- [38] Sun, S., He, Q., Xiao, S., Xu, Q., Li, X. and Zhou, L. 2012. Gradient-index meta-surfaces as a bridge linking propagating waves and surface waves. *Nature materials*, 11 (5), pp. 426--431.
- [39] Griffiths, D., 1999. *Introduction to electrodynamics*. 1st ed. Upper Saddle River, N.J.: Prentice Hall, pp.386-392.
- [40] Polyanskiy, M., 2013. *Refractive index of Silver (Ag) [CRYSTALS etc.] - RefractiveIndex.INFO*. [online]
- Refractiveindex.info. Available at:  
<http://refractiveindex.info/legacy/?group=METALS&material=Silver&option=Johnson&wavelength=0.635> [Accessed 21 Apr. 2014].
- [41] Johnson, P. and Christy, R., 1972. Optical constants of the noble metals. *Physical Review B*, 6(12), p.4370.
- [42] Polyanskiy, M., 2013. *Refractive index of Silver (Ag) [CRYSTALS etc.] - RefractiveIndex.INFO*. [online]
- Refractiveindex.info. Available at:  
<http://refractiveindex.info/legacy/?group=METALS&material=Silver&option=Johnson&wavelength=0.635> [Accessed 21 Apr. 2014].
- [43] Ciddor, P., 1996. Refractive index of air: new equations for the visible and near infrared. *Applied optics*, 35(9), pp.1566--1573.
- [44] Schneider, F., Draheim, J., Kammerer, R. and Wallrabe, U., 2009. Process and material properties of polydimethylsiloxane (PDMS) for Optical MEMS. *Sensors and Actuators A: Physical*, 151(2), pp.95--99.
- [45] Moliton, A., 2007. *Applied electromagnetism and materials*. 1st ed. New York, N.Y.: Springer. pp205-362.
- [46] Biacore.com, (2014). *Biacore Life Sciences > Technology > Introduction > Following an interaction*. [online] Available at:[https://www.biacore.com/lifesciences/technology/introduction/following\\_interaction/index.html](https://www.biacore.com/lifesciences/technology/introduction/following_interaction/index.html) [Accessed 23 Apr. 2014].